Aalto University

OPEN ACCESS

This is an electronic reprint of the original article.
This reprint may differ from the original in pagination and typographic detail.

Sayyad, Sharareh; Lado, Jose

Topological phase diagrams of exactly solvable non-Hermitian interacting Kitaev chains

Published in:
Physical Review Research

DOI:
10.1103/PhysRevResearch.5.L022046

Published: 02/06/2023

Document Version
Publisher's PDF, also known as Version of record

Published under the following license:
CC BY

Please cite the original version:
Sayyad, S., & Lado, J. (2023). Topological phase diagrams of exactly solvable non-Hermitian interacting Kitaev chains. *Physical Review Research*, *5*(2), 1-7. Article L022046.
https://doi.org/10.1103/PhysRevResearch.5.L022046

This material is protected by copyright and other intellectual property rights, and duplication or sale of all or part of any of the repository collections is not permitted, except that material may be duplicated by you for your research use or educational purposes in electronic or print form. You must obtain permission for any other use. Electronic or print copies may not be offered, whether for sale or otherwise to anyone who is not an authorised user.

Letter

Topological phase diagrams of exactly solvable non-Hermitian interacting Kitaev chains

Sharareh Sayyad [1,*] and Jose L. Lado[2]

[1]*Max Planck Institute for the Science of Light, Staudtstraße 2, 91058 Erlangen, Germany*

[2]*Department of Applied Physics, Aalto University, FI-00076 Aalto, Espoo, Finland*

(Received 6 March 2023; revised 11 May 2023; accepted 15 May 2023; published 2 June 2023)

Many-body interactions give rise to the appearance of exotic phases in Hermitian physics. Despite their importance, many-body effects remain an open problem in non-Hermitian physics due to the complexity of treating many-body interactions. Here, we present a family of exact and numerical phase diagrams for non-Hermitian interacting Kitaev chains. In particular, we establish the exact phase boundaries for the dimerized Kitaev-Hubbard chain with complex-valued Hubbard interactions. Our results reveal that some of the Hermitian phases disappear as non-Hermiticity is enhanced. Based on our analytical findings, we explore the regime of the model that goes beyond the solvable regime, revealing regimes where non-Hermitian topological degeneracy remains. The combination of our exact and numerical phase diagrams provides an extensive description of a family of non-Hermitian interacting models. Our results provide a stepping stone toward characterizing non-Hermitian topology in realistic interacting quantum many-body systems.

DOI: 10.1103/PhysRevResearch.5.L022046

Introduction. Many-body interactions play a crucial role in Hermitian quantum systems. The emergent correlation effects in these systems give rise to a variety of collective phenomena, such as spontaneous symmetry breaking [1–4], phase transitions [5–8], and the emergence of fractionalized quasiparticles [9–12]. Understanding these rich phenomena often requires the combination of analytical and numerical techniques due to the scarcity of exact solutions for many-body models. Nonetheless, especially in one-dimensional (1D) systems, analytical solutions in specific regimes are attainable [13–18]. Away from these parameter regimes, employing various numerical methods [13,19–25] allows the underlying physics of many-body systems in generic scenarios to be unveiled.

The presence of losses and dissipation in real systems provides natural platforms for realizing non-Hermitian models [26–36]. Non-Hermitian quantum models have arisen as a new paradigm to manipulate and interpret various emergent phenomena [37,38]. Here, non-Hermiticity emerges as the effective description [39–46] of out-of-equilibrium and open quantum systems, e.g., in superconducting qubits [47–49], giving rise to various phenomena absent in the Hermitian counterpart. Paradigmatic examples are the occurrence of various non-Hermitian degeneracies [50–54] and non-Hermitian (bulk) skin states [55,56]. Both of these phenomenologies are mainly explored in effectively single-particle non-Hermitian Hamiltonians, while non-Hermitian many-body effects have remained relatively unexplored, partly due to limitations of numerical methods [57–62]. In particular, recent efforts have addressed one-dimensional non-Hermitian fermionic [63–68] and bosonic [69,70] Hubbard models. Here, the non-Hermiticity is incorporated by having nonreciprocal hopping [63], complex hopping [65], or complex Hubbard interaction [64,66,67,71–73]. The latter form of non-Hermiticity provides effective descriptions for experiments on open quantum systems with two-body loss [74–77].

In this Research Letter, combining exact analytical results and numerical calculations, we establish the phase diagram of a family of non-Hermitian Kitaev chains [41,78–80]. Our interacting model consists of a complex-valued many-body interaction that may host Majorana modes, in particular, realizable in an array of Josephson junctions [81]. Our results reveal that, depending on the relative couplings, non-Hermitian interacting phases with topological degeneracies emerge in the system. We show how increasing the non-Hermiticity parameters affects some of the many-body topological phases. We furthermore present that the topological degeneracies of the model remain in the nonanalytically solvable regime by numerically solving the interacting problem.

Model. The Hamiltonian for the non-Hermitian dimerized Kitaev-Hubbard chain, schematically shown in Fig. 1, reads

$$\begin{aligned}\mathcal{H} = &-\sum_{j=1}^{L-1}[t_j(c_j^\dagger c_{j+1} + c_{j+1}^\dagger c_j) + \Delta_j(c_j^\dagger c_{j+1}^\dagger + c_{j+1}c_j)] \\ &+ \sum_{j=1}^{L-1}(U_j - i\delta_j)(2n_j - 1)(2n_{j+1} - 1) \\ &- \mu\sum_{j=1}^{L}\left(n_j - \frac{1}{2}\right), \end{aligned} \tag{1}$$

*shareareh.sayyad@mpl.mpg.de

Published by the American Physical Society under the terms of the Creative Commons Attribution 4.0 International license. Further distribution of this work must maintain attribution to the author(s) and the published article's title, journal citation, and DOI. Open access publication funded by the Max Planck Society.

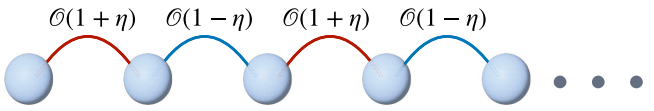

FIG. 1. Schematic illustration of a 1D dimerized Kitaev-Hubbard chain with dimerized hopping t, pairing Δ, and complex-valued Hubbard interaction $U - i\delta$. Here, η denotes the dimerization parameter, and $\mathcal{O} \in \{t, \Delta, U, \delta\}$.

where L denotes the length of the chain and $c_j^\dagger$ (c_j) creates (annihilates) a spinless fermion at site j associated with the fermion density $n_j = c_j^\dagger c_j$. Here, μ adjusts the on-site energy, and t_j, Δ_j, and U_j are the real-valued site-dependent hopping amplitude, superconducting pairing amplitude, and Hubbard interaction, respectively. The dimerized parameter $\mathcal{O}_j \in \{t_j, \Delta_j, U_j, \delta_j\}$ for $1 \leqslant j \leqslant L$ reads

$$\mathcal{O}_j = \begin{cases} \mathcal{O}(1-\eta), & j \bmod 2 = 0 \\ \mathcal{O}(1+\eta), & j \bmod 2 = 1, \end{cases} \tag{2}$$

where η is the real-valued dimerization parameter and $\mathcal{O} \in \{t, \Delta, U, \delta\}$ stands for site-independent parameters; see also Fig. 1. Considering such a form of dimerization for all parameters enables us to explore a family of Kitaev-Hubbard models but is mainly motivated by the limitation of obtaining exact solutions for our model. We note that despite dimerizing parameters, the system is still reciprocal; hence we do not expect the occurrence of the skin effect in our model.

The Hamiltonian in Eq. (1) at $\mu = 0$ remains invariant under $c_j \to (-1)^j c_j^\dagger$, which enforces the charge conjugation symmetry. We note that respecting this symmetry ensures that eigenvalues of the Hamiltonian come in complex-conjugate pairs making this model not directly realizable in open quantum systems [40], which can be resolved by a negative imaginary shift of all eigenvalues [82]. Nevertheless, preserving the charge conjugation symmetry in Hermitian models ($\delta = 0$) at the symmetric point $\Delta = t$ allows exact phase diagrams for arbitrary η to be calculated [13–17,83]. In the following, we present that there exists an analytical solution for the non-Hermitian model when the charge conjugation symmetry is respected, i.e., at $\mu = 0$ and $\Delta = t$. When $\Delta \neq t$ or $\mu \neq 0$, we compute the topological phase diagram numerically.

Exact solution at $\mu = 0$ and $\Delta = t$. To obtain the exact phase diagram of the model Hamiltonian at $\mu = 0$, we employ two Jordan-Wigner transformations and one spin rotation; see the Supplemental Material (SM) for details [84]. This procedure maps our initial non-Hermitian interacting Hamiltonian into a non-Hermitian quadratic fermionic model given by

$$\mathcal{H} = \sum_j -t_j[f_{j+1}^\dagger f_j + f_j^\dagger f_{j+1} + f_j^\dagger f_{j+1}^\dagger + f_{j+1} f_j] + \sum_j \tilde{U}_j[f_{j+1}^\dagger f_j + f_j^\dagger f_{j+1} - f_j^\dagger f_{j+1}^\dagger - f_{j+1} f_j], \tag{3}$$

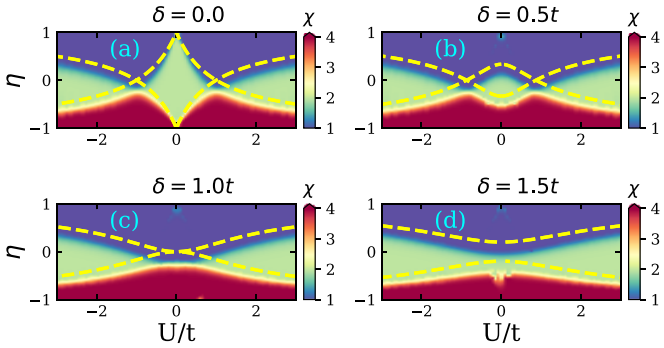

FIG. 2. Phase diagrams of the non-Hermitian Hamiltonian and associated orders of degeneracies on the $(U/t - \eta)$ plane at $\mu = 0$ and $\Delta = t$. The non-Hermiticity parameter is set to $\delta/t = 0$ (a), 0.5 (b), 1.0 (c), and 1.5 (d). The yellow dashed lines display the exact phase boundaries given by Eq. (6). The heat map shows the degeneracies obtained numerically for a chain with length $L = 16$, shown in red, green, and blue for fourfold, twofold, and no degeneracies, respectively.

which in the momentum space casts

$$\mathcal{H} = \sum_k (-t + \tilde{U})[z_k f_{kB}^\dagger f_{kA} + z_k^* f_{kA}^\dagger f_{kB}] - \sum_k (t + \tilde{U})[w_k f_{-kA}^\dagger f_{kB}^\dagger + w_k^* f_{kB} f_{-kA}], \tag{4}$$

where $\tilde{U} = U - i\delta$, $z_k = (1+\eta) + e^{-ika}(1-\eta)$, and $w_k = (1+\eta) - e^{-ika}(1-\eta)$. Diagonalizing this Hamiltonian, we obtain the energy spectrum of this four-band system given by

$$\frac{\Lambda_k^2}{4} = \begin{cases} \tilde{U}^2(1+\eta)^2 + t^2(1-\eta)^2 - 2t\tilde{U}(1-\eta^2)\cos(k) \\ \tilde{U}^2(1-\eta)^2 + t^2(1+\eta)^2 - 2t\tilde{U}(1-\eta^2)\cos(k), \end{cases} \tag{5}$$

where $\tilde{U}^2 = U^2 - \delta^2 - 2i\delta U$. As eigenvalues of our system appear in complex-conjugate pairs, due to the charge conjugation, zero modes in Λ_k emerge when $\mathrm{Re}[\Lambda_k] = 0$ at

$$\frac{U}{t} = \sqrt{\frac{\delta^2}{t^2} - \frac{(1 \pm \eta)^2}{(1 \mp \eta)^2}}, \tag{6}$$

which is obtained at $k = \pm\pi/2$. In the Hermitian limit ($\delta = 0$), Eq. (6) reproduces the Hermitian results [13–17]. Equation (6) shows the boundaries between various phases in our system, presented using yellow dashed lines in Fig. 2. These boundaries delineate phases with fourfold, twofold, and no degeneracies, respectively, shown in red, green, and blue in Fig. 2. The order of degeneracy is determined by $\chi = \sum_{i=0}^{L} \exp[-\lambda|\varepsilon_i - \varepsilon_0|]$. This quantity measures the degeneracy between the first eigenvalue ε_0 and the smallest eigenvalue ε_i within the energy resolution of $1/\lambda$ ($= 0.05$). Here, the eigenvalues are calculated using the numerical exact diagonalization method. The difference between the numerical boundaries and the exact solution should be attributed to the finite-size effect. In the thermodynamic limit ($L = \infty$), one can recover the exact phase boundaries; see the SM [84]. The topological superconducting phase residing in the boundaries surrounding $U = 0$ [85] shrinks as non-Hermiticity increases.

At the critical value $\delta = t$, this topological phase fades away, resulting in the mixing of other twofold degenerate phases. It is also worth noting that the exact phase boundaries in Eq. (6) are associated with transitions between non-Hermitian spectra with different types of gap in the non-Hermitian effective model in Eq. (4); see also the SM [84].

Many-body Majorana edge modes. To identify Majorana modes in our model, in the next step, we rewrite the Hamiltonian in Eq. (3) in terms of Majorana fermions $\Upsilon_j^A = f_j^\dagger + f_j$ and $\Upsilon_j^B = i(f_j^\dagger - f_j)$.The Hamiltonian then reads

$$\mathcal{H} = i\sum_j \left[t_j \Upsilon_j^B \Upsilon_{j+1}^A + \tilde{U}_j \Upsilon_j^A \Upsilon_{j+1}^B\right]. \tag{7}$$

We note that interactions and hopping amplitudes between the same sublattices or within each unit cell vanish. Hence Eq. (7) can be decoupled into two independent noninteracting Kitaev chains with length $L/2$ such that $\mathcal{H} = \mathcal{H}_{\rm I} + \mathcal{H}_{\rm II}$, where

$$\mathcal{H}_{\rm I} = \sum_{j=1}^{L/2}\left[-it_{2j}\Phi_{{\rm I},j+1}^A \Phi_{{\rm I},j}^B + i\tilde{U}_{2j-1}\Phi_{{\rm I},j}^A \Phi_{{\rm I},j}^B\right], \tag{8}$$

$$\mathcal{H}_{\rm II} = \sum_{j=1}^{L/2}\left[i\tilde{U}_{2j}\Phi_{{\rm II},j+1}^B \Phi_{{\rm II},j}^A - it_{2j-1}\Phi_{{\rm II},j}^B \Phi_{{\rm II},j}^A\right], \tag{9}$$

with $\Phi_{{\rm I},j}^A = \Upsilon_{2j-1}^A$, $\Phi_{{\rm I},j}^B = \Upsilon_{2j}^B$, $\Phi_{{\rm II},j}^B = \Upsilon_{2j-1}^B$, and $\Phi_{{\rm II},j}^B = \Upsilon_{2j}^A$. Introducing Majorana particles from the electron operators as $\gamma_j^A = c_j^\dagger + c_j$ and $\gamma_j^B = i(c_j^\dagger - c_j)$, one can show that Υ operators are products of γ operators such that [15,17,86–89]

$$\Upsilon_j^A = \begin{cases} \prod_{k=\rm odd}^{j-1}\left[i\gamma_k^B\gamma_{k+1}^A\right]\gamma_j^A, & j = \text{odd} \\ \prod_{k=\rm odd}^{j-3}\left[i\gamma_k^A\gamma_{k+1}^B\right](i\gamma_{j-1}^A\gamma_j^A), & j = \text{even}, \end{cases} \tag{10}$$

$$\Upsilon_j^B = \begin{cases} \prod_{k=\rm odd}^{j-2}\left[i\gamma_k^A\gamma_{k+1}^B\right]i\gamma_j^A\gamma_j^B, & j = \text{odd} \\ \prod_{k=\rm odd}^{j-1}\left[i\gamma_k^B\gamma_{k+1}^A\right]\gamma_j^B, & j = \text{even}. \end{cases} \tag{11}$$

These relations keep the Majorana anticommutation relations unchanged, i.e., $\{\Upsilon_i^\alpha, \Upsilon_j^\beta\} = \{\gamma_i^\alpha, \gamma_j^\beta\} = 2\delta_{i,j}\delta^{\alpha,\beta}$. We note that Υ operators which are composed of an odd (even) number of Majorana fermions (i.e., γ's) belong to subsystem I (II) described by $\mathcal{H}_{\rm I}$ ($\mathcal{H}_{\rm II}$).

The quadratic Hamiltonian in Eq. (7) may host two types of boundary modes ($\mathcal{Q}$). These boundary modes are constructed from linear combinations of $\Phi_{\rm I/II}^{A/B}$ operators, i.e., $\mathcal{Q}_\beta^\alpha = \sum_{j\geqslant 0} a_{\beta,j}\Phi_{\beta,j}^\alpha$ with $\alpha = A, B$ and $\beta = {\rm I}, {\rm II}$. As $\mathcal{Q}$ consists of higher-order multiple Majorana fermions, it is dubbed a "many-body Majorana operator" [89]. In the Hermitian limit, $\mathcal{Q}$ operators are conserved, $[\mathcal{H}, \mathcal{Q}] = 0$, and using the iteration procedure, one can determine the coefficients (a) as [15,89,90]

$$a_{{\rm I},j} = -\left(\frac{U(1+\eta)}{t(1-\eta)}\right)^{j-1}, \quad a_{{\rm II},j} = -\left(\frac{t(1+\eta)}{U(1-\eta)}\right)^{j-1}. \tag{12}$$

In non-Hermitian systems, the operator $\mathcal{O}$ is conserved if it satisfies $[\mathcal{H}_R, \mathcal{O}] = \{\mathcal{H}_{\rm I}, \mathcal{O}\} = 0$, where $\mathcal{H} = \mathcal{H}_R + i\mathcal{H}_{\rm I}$ [54]. We note that based on the structure of $\mathcal{H}_{\rm I}$ and $\mathcal{H}_{\rm II}$ in Eqs. (8) and (9), $\{\mathcal{H}_{\rm I}, \mathcal{O}\} = 0$ is by construction satisfied and fulfilling $[\mathcal{H}_R, \mathcal{O}] = 0$ results in obtaining Eq. (12). Hence the boundary modes in our non-Hermitian system are continuously ($\delta \to 0$) connected to the zero-energy boundary modes.

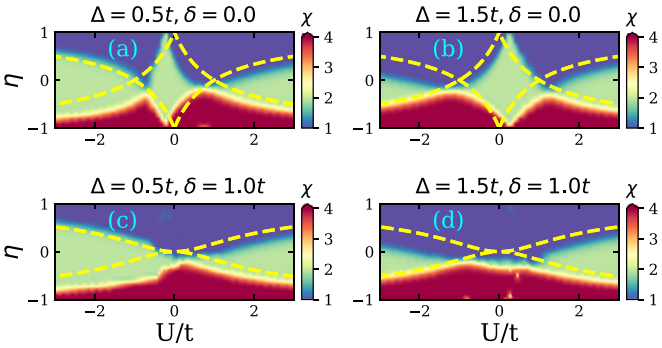

FIG. 3. Phase diagrams of the non-Hermitian Hamiltonian and associated orders of degeneracies on the $(U/t - \eta)$ plane at $\mu = 0$ and $\Delta \neq t$. The heat map corresponds to the degeneracies obtained numerically for a system with $L = 16$. The superconducting pairing amplitude and non-Hermiticity are set to $(\Delta/t, \delta) =$ (0.5, 0.0) (a), (1.5,0.0) (b), (0.5,1.0) (c), and (1.5,1.0) (d). The yellow dashed lines are phase boundaries at $\Delta = t$ and are shown as a guide for the eye.

The Majorana boundary mode $\mathcal{Q}_{\rm I}$ consists of odd numbers of higher-order Majorana operators (γ), is fermionic, and satisfies $\{\mathcal{Z}_2, \mathcal{Q}_{\rm I}\} = 0$, with $\mathcal{Z}_2$ being the fermion parity operator $\mathcal{Z}_2 = (-1)^{\sum_j c_j^\dagger c_j}$, in the infinite-chain limit [90]. However, the $\mathcal{Q}_{\rm II}$ mode comprises even numbers of higher-order Majorana operators (γ) and is bosonic as $[\mathcal{Z}_2, \mathcal{Q}_{\rm II}] = 0$ [14,15,89]. Regions with fourfold degeneracies in Fig. 2 host both ($\mathcal{Q}_{\rm I}, \mathcal{Q}_{\rm II}$). The topological superconducting phase enclosing $U = 0$ merely hosts $\mathcal{Q}_{\rm I}$, in agreement with Hermitian noninteracting intuition [85]. The other two twofold degenerate phases accommodate $\mathcal{Q}_{\rm II}$.

Beyond exact solutions. Let us now present the phase diagram of our system away from the integrable regime $\Delta = t$ and $\mu = 0$. First, we consider $\Delta/t \in \{0.5, 1.5\}$ and plot the associated phase diagrams with $\delta \in \{0.0, 1.0\}$ in Fig. 3 for a finite-size system with $L = 16$. Similar to the phase diagram of the system at $\Delta = t$, we witness phases with fourfold, twofold, and no degeneracies. Comparing the exact phase boundaries at $\Delta = t$, in yellow dashed lines, with boundaries of regions with $2n$-fold degeneracies, in red or green, we identify deformation of the phase boundaries toward $U < 0$ (>0) for $\Delta < t$ ($> t$).

At finite chemical potential and $\delta = 0$, all fourfold degeneracies are lifted, and merely phases with twofold degeneracies remain in the phase diagram; see Fig. 4. The Hermitian phase boundary $U = -0.5t$ at $\eta = 0$ is consistent with previous calculations on the Kitaev-Hubbard chain [91]; see Fig. 4(a) at $L = 16$, Fig. 4(c) in the thermodynamics limit, and the SM [84]. Witnessing merely twofold degeneracies in phases with $U > 1$ in the Hermitian limit also persists as non-Hermiticity is increased; see Fig. 4(b) at $L = 16$. While no portion of the topological superconducting phase, the region encircling $U = 0$, is present in Fig. 4(b) obtained at $\mu = 0.25$ and $L = 16$, extrapolating the phase diagram using different

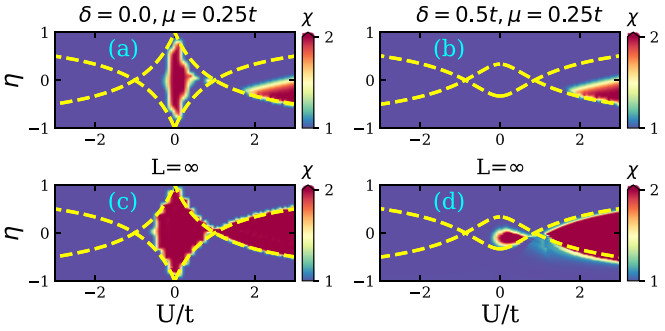

FIG. 4. Phase diagrams of the non-Hermitian Hamiltonian and associated orders of degeneracies on the $(U/t - \eta)$ plane with $\mu \neq 0$. The superconducting pairing amplitude is set to $\Delta = t$. The chain size is set to $L = 16$ in (a) and (b), and extrapolated data in the thermodynamic limit are shown in (c) and (d). The yellow dashed lines are phase boundaries at $\mu = 0$ and are shown as a guide for the eye. We took $\delta, \mu = 0, 0.25t$ in (a) and (c) and $\delta, \mu = 0.5, 0.25t$ in (b) and (d).

system sizes, shown in Fig. 4(d), reveals the survival of this phase at $L = \infty$.

Experimental measurement. We now address the signatures of the zero modes from the experimental point of view. In a tunneling experiment with a local probe [92–96], the conductance at zero bias $G(\omega = 0, n)$ depends on the probability of extracting (injecting) an electron in site n at energy ω as $dI/dV(n, \omega) \sim \sum_\alpha |\langle \mathrm{GS}|c_n^{(\dagger)}|\Psi_\alpha\rangle|^2 \delta(\omega - E_\alpha + E_{\mathrm{GS}})$, where $|\mathrm{GS}\rangle$ is the ground state and $H|\Psi_\alpha\rangle = E_\alpha|\Psi_\alpha\rangle$ are the many-body excited states of the system. In the presence of topological degeneracy, the ground state presents zero-mode excitations that distinguish different ground states. In that scenario, the zero-bias conductance at site n can be written as $dI/dV(n, \omega = 0) \sim \Xi(n)$, where

$$\Xi(n) = \sum_\alpha |\langle \Psi_\alpha|c_n|\mathrm{GS}\rangle|^2 + |\langle \Psi_\alpha|c_n^\dagger|\mathrm{GS}\rangle|^2, \qquad (13)$$

which directly images the probability of a local excitation between the ground state and its degenerate manifold. Here, α runs over the ground state manifold. In particular, $\Xi(n)$ allows one to directly observe the emergence of topological zero modes associated with the topological degeneracy of the ground state. With the previous quantity, the emergence of topological zero modes associated with the topological degeneracy of the non-Hermitian model can be directly imaged. We show in Fig. 5 the local correlator computed for the interacting non-Hermitian model for different system sizes. As the system becomes larger, an edge excitation emerges in the model, which in the thermodynamic limit leads to decoupled modes between the two edges; see also the SM [84]. The previous quantity has been directly imaged in the realization of the current model in the topological phase with $\delta = U = 0$ and $\eta \neq 0$ [92], and a minimal chain with $\Delta \neq 0$ [96].

Conclusion. To summarize, we have presented a family of non-Hermitian interacting models featuring different classes of topological degeneracies. While noninteracting non-Hermitian models can be studied with conventional methodologies, the inclusion of many-body interactions renders exploring non-Hermitian systems greatly challenging. This Research Letter establishes a family of solvable interacting non-Hermitian models, providing ideal systems for benchmarking methodologies to treat interacting non-Hermitian models. Besides showing the emergence of different topological phases in the solvable limit, we provided the many-body operators accounting for the topological degeneracy of the model. We showed how non-Hermiticity modifies topological many-body models, substantially impacting the topological phases of Hermitian systems. We benchmarked our analytical construction with exact numerical calculations of the full many-body system, demonstrating that even for finite systems, the emergence of topological modes and topological degeneracies can be observed. Our results establish a versatile family of models featuring interacting topology, providing a starting point for higher-dimensional solvable interacting models.

Acknowledgments. S.S. thanks Vittorio Paeno and Abolhassan Vaezi for helpful discussions. J.L.L. acknowledges the computational resources provided by the Aalto Science-IT project and the financial support from Academy of Finland Projects No. 331342 and No. 336243 and the Jane and Aatos Erkko Foundation.

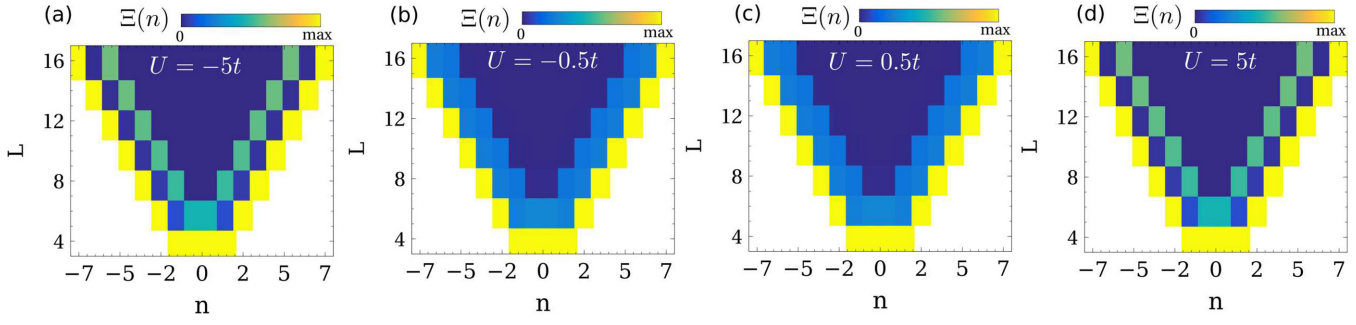

FIG. 5. Spatial distribution of the zero modes for different system lengths for the non-Hermitian model computed with the local response function given by Eq. (13). It is observed that both in the presence of repulsive interactions and in the presence of attractive interactions, an edge response appears, accounting for the topological degeneracy of the model. The edge excitations emerge both in the case of twofold [(a) and (d)] and fourfold [(b) and (c)] degeneracy. We took $\mu = 0$, $\Delta = t$, $\eta = -0.6$, and $\delta = 0.5t$.

[1] T. Koma and H. Tasaki, Symmetry breaking and finite-size effects in quantum many-body systems, J. Stat. Phys. **76**, 745 (1994).

[2] S. T. Belyaev, Many-body physics and spontaneous symmetry breaking, Int. J. Mod. Phys. B **20**, 2579 (2006).

[3] T. Brauner, Spontaneous symmetry breaking and Nambu-Goldstone bosons in quantum many-body systems, Symmetry **2**, 609 (2010).

[4] G.-H. Dong, Y.-N. Fang, and C.-P. Sun, Quantifying spontaneously symmetry breaking of quantum many-body systems, Commun. Theor. Phys. **68**, 405 (2017).

[5] L. F. Santos, M. Távora, and F. Pérez-Bernal, Excited-state quantum phase transitions in many-body systems with infinite-range interaction: Localization, dynamics, and bifurcation, Phys. Rev. A **94**, 012113 (2016).

[6] M. Heyl, Dynamical quantum phase transitions: A review, Rep. Prog. Phys. **81**, 054001 (2018).

[7] A. Carollo, D. Valenti, and B. Spagnolo, Geometry of quantum phase transitions, Phys. Rep. **838**, 1 (2020).

[8] T. Serwatka, R. G. Melko, A. Burkov, and P.-N. Roy, Quantum Phase Transition in the One-Dimensional Water Chain, Phys. Rev. Lett. **130**, 026201 (2023).

[9] G.-Q. Zhang, D.-W. Zhang, Z. Li, Z. D. Wang, and S.-L. Zhu, Statistically related many-body localization in the one-dimensional anyon Hubbard model, Phys. Rev. B **102**, 054204 (2020).

[10] M. Hashisaka, T. Jonckheere, T. Akiho, S. Sasaki, J. Rech, T. Martin, and K. Muraki, Andreev reflection of fractional quantum Hall quasiparticles, Nat. Commun. **12**, 2794 (2021).

[11] V. Kaskela and J. L. Lado, Dynamical topological excitations in parafermion chains, Phys. Rev. Res. **3**, 013095 (2021).

[12] J. Wouters, F. Hassler, H. Katsura, and D. Schuricht, Phase diagram of an extended parafermion chain, SciPost Phys. Core **5**, 008 (2022).

[13] S. Gangadharaiah, B. Braunecker, P. Simon, and D. Loss, Majorana Edge States in Interacting One-Dimensional Systems, Phys. Rev. Lett. **107**, 036801 (2011).

[14] H. Katsura, D. Schuricht, and M. Takahashi, Exact ground states and topological order in interacting Kitaev/Majorana chains, Phys. Rev. B **92**, 115137 (2015).

[15] M. Ezawa, Exact solutions and topological phase diagram in interacting dimerized Kitaev topological superconductors, Phys. Rev. B **96**, 121105(R) (2017).

[16] Y. Wang, J. J. Miao, H. K. Jin, and S. Chen, Characterization of topological phases of dimerized Kitaev chain via edge correlation functions, Phys. Rev. B **96**, 205428 (2017).

[17] J.-J. Miao, H.-K. Jin, F.-C. Zhang, and Y. Zhou, Exact Solution for the Interacting Kitaev Chain at the Symmetric Point, Phys. Rev. Lett. **118**, 267701 (2017).

[18] A. A. Zvyagin, Charging of Majorana edge modes caused by interaction: Exact results, Phys. Rev. B **105**, 115406 (2022).

[19] H. Q. Lin, Exact diagonalization of quantum-spin models, Phys. Rev. B **42**, 6561 (1990).

[20] G. Vidal, Efficient Simulation of One-Dimensional Quantum Many-Body Systems, Phys. Rev. Lett. **93**, 040502 (2004).

[21] U. Schollwöck, The density-matrix renormalization group, Rev. Mod. Phys. **77**, 259 (2005).

[22] G. Kotliar, S. Y. Savrasov, K. Haule, V. S. Oudovenko, O. Parcollet, and C. A. Marianetti, Electronic structure calculations with dynamical mean-field theory, Rev. Mod. Phys. **78**, 865 (2006).

[23] E. M. Stoudenmire, J. Alicea, O. A. Starykh, and M. P. A. Fisher, Interaction effects in topological superconducting wires supporting majorana fermions, Phys. Rev. B **84**, 014503 (2011).

[24] P. Silvi, F. Tschirsich, M. Gerster, J. Jünemann, D. Jaschke, M. Rizzi, and S. Montangero, The tensor networks anthology: Simulation techniques for many-body quantum lattice systems, SciPost Phys. Lect. Notes 8 (2019).

[25] R. Tuovinen, Electron correlation effects in superconducting nanowires in and out of equilibrium, New J. Phys. **23**, 083024 (2021).

[26] K. Esaki, M. Sato, K. Hasebe, and M. Kohmoto, Edge states and topological phases in non-hermitian systems, Phys. Rev. B **84**, 205128 (2011).

[27] S. Malzard, C. Poli, and H. Schomerus, Topologically Protected Defect States in Open Photonic Systems with Non-Hermitian Charge-Conjugation and Parity-Time Symmetry, Phys. Rev. Lett. **115**, 200402 (2015).

[28] Z. Gong, Y. Ashida, K. Kawabata, K. Takasan, S. Higashikawa, and M. Ueda, Topological Phases of Non-Hermitian Systems, Phys. Rev. X **8**, 031079 (2018).

[29] S. Yao and Z. Wang, Edge States and Topological Invariants of Non-Hermitian Systems, Phys. Rev. Lett. **121**, 086803 (2018).

[30] H. Shen, B. Zhen, and L. Fu, Topological Band Theory for Non-Hermitian Hamiltonians, Phys. Rev. Lett. **120**, 146402 (2018).

[31] K. Kawabata, K. Shiozaki, M. Ueda, and M. Sato, Symmetry and Topology in Non-Hermitian Physics, Phys. Rev. X **9**, 041015 (2019).

[32] K. Yokomizo and S. Murakami, Non-Bloch Band Theory of Non-Hermitian Systems, Phys. Rev. Lett. **123**, 066404 (2019).

[33] H. Zhou and J. Y. Lee, Periodic table for topological bands with non-Hermitian symmetries, Phys. Rev. B **99**, 235112 (2019).

[34] D. S. Borgnia, A. J. Kruchkov, and R.-J. Slager, Non-Hermitian Boundary Modes and Topology, Phys. Rev. Lett. **124**, 056802 (2020).

[35] Y. Ashida, Z. Gong, and M. Ueda, Non-Hermitian physics, Adv. Phys. **69**, 249 (2020).

[36] K. Yang, S. C. Morampudi, and E. J. Bergholtz, Exceptional Spin Liquids from Couplings to the Environment, Phys. Rev. Lett. **126**, 077201 (2021).

[37] S. Sayyad, J. D. Hannukainen, and A. G. Grushin, Non-Hermitian chiral anomalies, Phys. Rev. Res. **4**, L042004 (2022).

[38] N. Okuma and M. Sato, Non-Hermitian topological phenomena: A review, Annu. Rev. Condens. Matter Phys. **14**, 83 (2023).

[39] T. Prosen, Third quantization: A general method to solve master equations for quadratic open Fermi systems, New J. Phys. **10**, 043026 (2008).

[40] S. Lieu, M. McGinley, and N. R. Cooper, Tenfold Way for Quadratic Lindbladians, Phys. Rev. Lett. **124**, 040401 (2020).

[41] S. Sayyad, J. Yu, A. G. Grushin, and L. M. Sieberer, Entanglement spectrum crossings reveal non-Hermitian dynamical topology, Phys. Rev. Res. **3**, 033022 (2021).

[42] J. Perina Jr, A. Miranowicz, G. Chimczak, and A. Kowalewska-Kudlaszyk, Quantum Liouvillian exceptional and diabolical points for bosonic fields with quadratic Hamiltonians: The Heisenberg-Langevin equation approach, Quantum **6**, 883 (2022).

[43] F. Yang, Q.-D. Jiang, and E. J. Bergholtz, Liouvillian skin effect in an exactly solvable model, Phys. Rev. Res. **4**, 023160 (2022).

[44] S. Talkington and M. Claassen, Dissipation-induced flat bands, Phys. Rev. B **106**, L161109 (2022).

[45] E. Starchl and L. M. Sieberer, Relaxation to a Parity-Time Symmetric Generalized Gibbs Ensemble after a Quantum Quench in a Driven-Dissipative Kitaev Chain, Phys. Rev. Lett. **129**, 220602 (2022).

[46] C. Gneiting, A. Koottandavida, A. V. Rozhkov, and F. Nori, Unraveling the topology of dissipative quantum systems, Phys. Rev. Res. **4**, 023036 (2022).

[47] W. Chen, M. Abbasi, Y. N. Joglekar, and K. W. Murch, Quantum Jumps in the Non-Hermitian Dynamics of a Superconducting Qubit, Phys. Rev. Lett. **127**, 140504 (2021).

[48] M. Abbasi, W. Chen, M. Naghiloo, Y. N. Joglekar, and K. W. Murch, Topological Quantum State Control through Exceptional-Point Proximity, Phys. Rev. Lett. **128**, 160401 (2022).

[49] W. Chen, M. Abbasi, B. Ha, S. Erdamar, Y. N. Joglekar, and K. W. Murch, Decoherence-Induced Exceptional Points in a Dissipative Superconducting Qubit, Phys. Rev. Lett. **128**, 110402 (2022).

[50] D. Leykam, K. Y. Bliokh, C. Huang, Y. D. Chong, and F. Nori, Edge Modes, Degeneracies, and Topological Numbers in Non-Hermitian Systems, Phys. Rev. Lett. **118**, 040401 (2017).

[51] E. J. Bergholtz, J. C. Budich, and F. K. Kunst, Exceptional topology of non-Hermitian systems, Rev. Mod. Phys. **93**, 015005 (2021).

[52] S. Sayyad and F. K. Kunst, Realizing exceptional points of any order in the presence of symmetry, Phys. Rev. Res. **4**, 023130 (2022).

[53] S. Sayyad, M. Stalhammar, L. Rodland, and F. K. Kunst, Symmetry-protected exceptional and nodal points in non-Hermitian systems, arXiv:2204.13945.

[54] S. Sayyad, Protection of all nondefective twofold degeneracies by antiunitary symmetries in non-Hermitian systems, Phys. Rev. Res. **4**, 043213 (2022).

[55] F. Song, S. Yao, and Z. Wang, Non-Hermitian Skin Effect and Chiral Damping in Open Quantum Systems, Phys. Rev. Lett. **123**, 170401 (2019).

[56] X. Zhang, T. Zhang, M.-H. Lu, and Y.-F. Chen, A review on non-Hermitian skin effect, Adv. Phys.: X **7**, 2109431 (2022).

[57] R. W. Freund, Quasi-kernel polynomials and their use in non-Hermitian matrix iterations, J. Comput. Appl. Math. **43**, 135 (1992).

[58] R. W. Freund, M. H. Gutknecht, and N. M. Nachtigal, An implementation of the look-ahead Lanczos algorithm for non-Hermitian matrices, SIAM J. Sci. Comput. **14**, 137 (1993).

[59] Z. Guo, Z.-T. Xu, M. Li, L. You, and S. Yang, Variational matrix product state approach for non-Hermitian system based on a companion Hermitian Hamiltonian, arXiv:2210.14858.

[60] R. Carden, Ritz values and Arnoldi convergence for non-Hermitian matrices, Ph.D. thesis, Rice University, 2011.

[61] J. Zhang and H. Dai, Global GPBiCG method for complex non-Hermitian linear systems with multiple right-hand sides, Comput. Appl. Math. **35**, 171 (2016).

[62] G. Chen, F. Song, and J. L. Lado, Topological Spin Excitations in Non-Hermitian Spin Chains with a Generalized Kernel Polynomial Algorithm, Phys. Rev. Lett. **130**, 100401 (2022).

[63] T. Fukui and N. Kawakami, Breakdown of the Mott insulator: Exact solution of an asymmetric Hubbard model, Phys. Rev. B **58**, 16051 (1998).

[64] B. Buča, C. Booker, M. Medenjak, and D. Jaksch, Bethe ansatz approach for dissipation: Exact solutions of quantum many-body dynamics under loss, New J. Phys. **22**, 123040 (2020).

[65] X. Z. Zhang and Z. Song, η-pairing ground states in the non-Hermitian Hubbard model, Phys. Rev. B **103**, 235153 (2021).

[66] M. Nakagawa, N. Kawakami, and M. Ueda, Exact Liouvillian Spectrum of a One-Dimensional Dissipative Hubbard Model, Phys. Rev. Lett. **126**, 110404 (2021).

[67] H. Yoshida and H. Katsura, Liouvillian gap and single spin-flip dynamics in the dissipative Fermi-Hubbard model, Phys. Rev. A **107**, 033332 (2023).

[68] T. Hyart and J. L. Lado, Non-Hermitian many-body topological excitations in interacting quantum dots, Phys. Rev. Res. **4**, L012006 (2022).

[69] K. Yamamoto, M. Nakagawa, M. Tezuka, M. Ueda, and N. Kawakami, Universal properties of dissipative Tomonaga-Luttinger liquids: Case study of a non-Hermitian XXZ spin chain, Phys. Rev. B **105**, 205125 (2022).

[70] Y.-N. Wang, W.-L. You, and G. Sun, Quantum criticality in interacting bosonic Kitaev-Hubbard models, Phys. Rev. A **106**, 053315 (2022).

[71] K. Yamamoto, M. Nakagawa, K. Adachi, K. Takasan, M. Ueda, and N. Kawakami, Theory of Non-Hermitian Fermionic Superfluidity with a Complex-Valued Interaction, Phys. Rev. Lett. **123**, 123601 (2019).

[72] M. Nakagawa, N. Tsuji, N. Kawakami, and M. Ueda, Dynamical Sign Reversal of Magnetic Correlations in Dissipative Hubbard Models, Phys. Rev. Lett. **124**, 147203 (2020).

[73] K. Yamamoto and N. Kawakami, Universal description of dissipative Tomonaga-Luttinger liquids with SU(N) spin symmetry: Exact spectrum and critical exponents, Phys. Rev. B **107**, 045110 (2023).

[74] M. Lewenstein, A. Sanpera, V. Ahufinger, B. Damski, A. Sen(De), and U. Sen, Ultracold atomic gases in optical lattices: Mimicking condensed matter physics and beyond, Adv. Phys. **56**, 243 (2007).

[75] Q. Zhang, M. Lou, X. Li, J. L. Reno, W. Pan, J. D. Watson, M. J. Manfra, and J. Kono, Collective non-perturbative coupling of 2D electrons with high-quality-factor terahertz cavity photons, Nat. Phys. **12**, 1005 (2016).

[76] C. Gross and I. Bloch, Quantum simulations with ultracold atoms in optical lattices, Science **357**, 995 (2017).

[77] L. Rosso, L. Mazza, and A. Biella, Eightfold way to dark states in SU(3) cold gases with two-body losses, Phys. Rev. A **105**, L051302 (2022).

[78] D. Rainis and D. Loss, Majorana qubit decoherence by quasiparticle poisoning, Phys. Rev. B **85**, 174533 (2012).

[79] S. Lieu, Non-Hermitian Majorana modes protect degenerate steady states, Phys. Rev. B **100**, 085110 (2019).

[80] T. Sakaguchi, H. Nishijima, and Y. Takane, Bulk–boundary correspondence and boundary zero modes in a non-Hermitian Kitaev chain model, J. Phys. Soc. Jpn. **91**, 124711 (2022).

[81] F. Hassler and D. Schuricht, Strongly interacting Majorana modes in an array of Josephson junctions, New J. Phys. **14**, 125018 (2012).

[82] Y. N. Joglekar and A. K. Harter, Passive parity-time-symmetry-breaking transitions without exceptional points in dissipative photonic systems, Photon. Res. **6**, A51 (2018).

[83] G. Y. Chitov, Local and nonlocal order parameters in the Kitaev chain, Phys. Rev. B **97**, 085131 (2018).

[84] See Supplemental Material at http://link.aps.org/supplemental/10.1103/PhysRevResearch.5.L022046 for details about mapping the non-Hermitian interacting Kitaev chain into a noninteracting Hamiltonian and discussions on the thermodynamic limits of topological modes and topological boundaries.

[85] A. Y. Kitaev, Unpaired Majorana fermions in quantum wires, Phys. Usp. **44**, 131 (2001).

[86] G. Goldstein and C. Chamon, Exact zero modes in closed systems of interacting fermions, Phys. Rev. B **86**, 115122 (2012).

[87] G. Yang and D. E. Feldman, Exact zero modes and decoherence in systems of interacting Majorana fermions, Phys. Rev. B **89**, 035136 (2014).

[88] G. Kells, Multiparticle content of Majorana zero modes in the interacting *p*-wave wire, Phys. Rev. B **92**, 155434 (2015).

[89] M. McGinley, J. Knolle, and A. Nunnenkamp, Robustness of Majorana edge modes and topological order: Exact results for the symmetric interacting Kitaev chain with disorder, Phys. Rev. B **96**, 241113(R) (2017).

[90] P. Fendley, Parafermionic edge zero modes in Zn-invariant spin chains, J. Stat. Mech.: Theory Exp. (2012) P11020.

[91] I. Mahyaeh and E. Ardonne, Study of the phase diagram of the Kitaev-Hubbard chain, Phys. Rev. B **101**, 085125 (2020).

[92] R. Drost, T. Ojanen, A. Harju, and P. Liljeroth, Topological states in engineered atomic lattices, Nat. Phys. **13**, 668 (2017).

[93] S. N. Kempkes, M. R. Slot, J. J. van den Broeke, P. Capiod, W. A. Benalcazar, D. Vanmaekelbergh, D. Bercioux, I. Swart, and C. Morais Smith, Robust zero-energy modes in an electronic higher-order topological insulator, Nat. Mater. **18**, 1292 (2019).

[94] S. N. Kempkes, M. R. Slot, S. E. Freeney, S. J. M. Zevenhuizen, D. Vanmaekelbergh, I. Swart, and C. Morais Smith, Design and characterization of electrons in a fractal geometry, Nat. Phys. **15**, 127 (2019); **17**, 1066(E) (2021).

[95] M. N. Huda, S. Kezilebieke, T. Ojanen, R. Drost, and P. Liljeroth, Tuneable topological domain wall states in engineered atomic chains, npj Quantum Mater. **5**, 17 (2020).

[96] T. Dvir, G. Wang, N. van Loo, C.-X. Liu, G. P. Mazur, A. Bordin, S. L. D. ten Haaf, J.-Y. Wang, D. van Driel, F. Zatelli, X. Li, F. K. Malinowski, S. Gazibegovic, G. Badawy, E. P. A. M. Bakkers, M. Wimmer, and L. P. Kouwenhoven, Realization of a minimal Kitaev chain in coupled quantum dots, Nature (London) **614**, 445 (2023).